# Sloshing and scaling: experimental study in a wave canal at two different scales

*O. Kimmoun* [(1)], *A. Ratouis* [(2)], *L. Brosset* [(2)]
[(1)]Ecole Centrale Marseille
Marseille, France
[(2)]Liquid motion dept, Gaztransport & Technigaz
Saint-Rémy-lès-Chevreuse, France

## ABSTRACT

Sloshing model tests are the basis of any sloshing assessment for a new membrane LNG carrier project. The statistical pressure results have to be scaled to full scale in order to derive design loads. The approach for scaling is not obvious as multi-physics occur within the impacts.

Experimental modeling is based on the Froude scaling assumption: if the forced motions at small scale are defined with a geometrical scale $1/\lambda$ and a time scale $1/\sqrt{\lambda}$, the velocities in both fluids, liquid and gas, should be in Froude accordance at both scales. This is exact for the *global flow* but Braeunig *et al*., (2009) have shown that it is wrong locally during the sloshing impacts, even though the density ratio between the fluids are kept the same at both scales, because the speeds of sound in the model liquid and gas are not in Froude accordance with the speeds of sound of respectively LNG and natural gas. The study presented here is an experimental attempt to show evidence of this so-called *compressibility bias* of sloshing experimental modeling.

Performing sloshing tests with model tanks at two different scales would have led only to a statistical comparison of the impact pressures. In order to have a direct deterministic comparison of Froude-similar liquid impacts on a wall at two different scales, the study deals with single breaking waves in a laboratory wave canal at two different scales referred to as scales $s_1$ and $s_{1/2}$.

After describing the experimental set-up and the breaking wave generation process, the paper shows the difficulties to reproduce accurately local developments of the impacts and the significant consequences of light discrepancies on the pressures. At the end the study describes how a relatively good similarity between flows at the two scales is obtained. A global analysis shows the general trend of the scaling for the pressures inside gas pockets.

KEY WORDS: Sloshing, Liquid Impact, Breaking Waves, Flume tank, Experiments, scaling, Froude, Compressibility, LNG carriers

## INTRODUCTION

Repeating sloshing model tests leads to a large scattering of the impact pressures in the sample. Only after a statistical post-processing of long duration tests, allowing for a large sample, will the pressure results become reasonably repeatable. The origin of the scattering of impact pressure is commonly attributed to local phenomena while the global flow is considered as quasi-deterministically defined. The scattering which is also a lack of repeatability can be attributed to the complex turbulent and three-dimensional flows. It makes sense that studying a single two-dimensional breaking wave should lead to a better repeatability. Reproducing two flows at two different geometrical scales consists in imposing Froude-scaled excitations to a liquid. According to waves equations the global flow (velocities) remains the same after Froude-scaling. What happens locally around each impact area (the local flow), during a very short duration starting with the compression of the escaping gas, is more complex and involves multi-physics including gas compressibility effects. For realistic impacts, the physics local phenomena should occur with the same intensity at both scales. The transfer of momentum between gas and liquid is one of the phenomena and is governed by the ratio of densities between gas and liquid. Keeping the same density ratio at both scales takes off a bias source between the scales. Thus, it allows for the studying of other sources of differences. The principle remaining source of bias is then compressibility effects. Other sources could be mentioned such as phase transition or different hydro-elastic effects.

The objective of the study presented in this paper is to compare deterministically local fluid impact pressures obtained experimentally at two different scales for similar Froude-scaled global flows. This objective leads directly to different pre-requirements:

1. Ensure that, at each scale, the global flow is repeatable when repeating carefully the same wave maker signal
2. Ensure that, at each scale, local impact pressure measurements are repeatable when repeating carefully the same global flow
3. Ensure that the experimental set-up allows a good similarity of the global flows at the two scales for the different conditions studied

The paper explains which precautions are necessary to achieve these requirements.

The experimental facility selected is the ~17 m laboratory flume tank of *Ecole Centrale Marseille* (ECM) (Kimmoun *et al*., 2009). A flap-type wave maker generates idealized, unidirectional breaking waves by a focusing process. The waves focus at a selected distance of the flap and impact an instrumented rigid wall when breaking.

## TEST SET-UP AND BREAKING WAVE GENERATION

Two scales are studied with a geometrical ratio of ½ in all directions. They are referred to as scale $s_1$ and $s_{1/2}$. Thanks to a movable test wall, the set-up is adapted for dealing with the two scales. At both scales, the distances between the wave maker and the wall, the liquid heights in the canal, the locations of the pressure sensors with regards to the free surface at rest are geometrically scaled and the wave maker signals are both geometrically and time scaled in order to be in a *Froude* similarity. Only the size and the density of the pressure sensors on the wall remain the same at both scales.

## Flume tank

The wave tank is 16.77 m long. A rotational wave maker is installed at an end. At the other end the instrumented wall is located at $D_1$ = 15.5 m from the flap at scale $s_1$ and at $D_{1/2}$ = 7.75 m at scale $s_{1/2}$. The longitudinal walls are transparent sections of glass supported by metallic frames. The movable flap and a horizontal bottom lay above the fix concrete floor of the room. Figure 1 and Figure 2 show schematically the installation and the main dimensions at both scales.

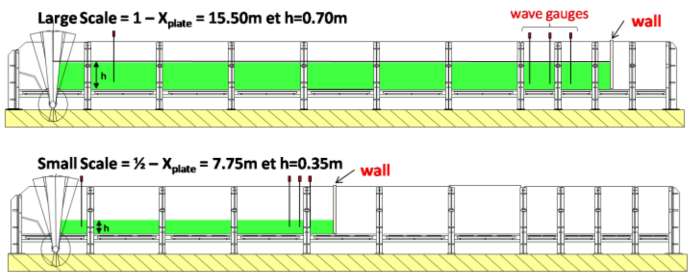


**Fig.1** - Schematic description of the wave canal at both scales

During the whole study, except a specific sensitivity study on the water depth, the water depth at rest was fixed to $h_1$ = 0.7 m at scale $s_1$ and $h_{1/2}$ = 0.35 m at scale $s_{1/2}$.

## Instrumentation

- Four resistive wave gauges referred to as wg1, wg2, wg3, wg4 are installed in the first part of the canal. The distances from the wave maker are given in table 1.

**Table 1** – distance from the flap to the wave gauges at both scales

| | $wg_1$ (m) | $wg_2$ (m) | $wg_3$ (m) | $wg_4$ (m) |
|---|---|---|---|---|
| **Scale $s_1$** | 1.65 | 13.1 | 13.45 | 13.85 |
| **Scale $s_{1/2}$** | 0.825 | 6.55 | 6.725 | 6.925 |

- Two capacitive wire sticks are glued on the movable test wall in order to measure accurately the run-up of the waves along the wall after impacting. Their location on both sides of the wall is shown in Figure 2.

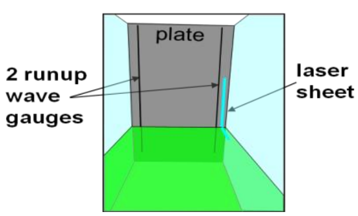


**Fig.2** – Locations of run-up wave gauges and laser sheet for PIV

- 88 PCB pressure transducers are screwed in two metallic modules inserted in the wall. The PCB sensors are piezo-electric. They have a sensitive circular area of 5.5 mm diameter.
- The same two metallic modules are used at both scales enabling setting a hundred sensors. The two modules are identical. Their positions on the test wall at both scales with regards to the water free surface at rest are shown in Figure 3. The sensors are mainly arranged on horizontal and vertical lines. The minimum distance between two sensors on these lines is 1 cm. In the main area of interest (close to the impact zone), the lines of sensors have been doubled in a staggered way so that, assuming the flow is perfectly 2D, a measurement every 5 mm in both directions is possible. A zoom-in in Figure 3 shows this sensor arrangement.
- The data acquisition is performed by a National Instruments PXI system with a sampling frequency at 40 kHz

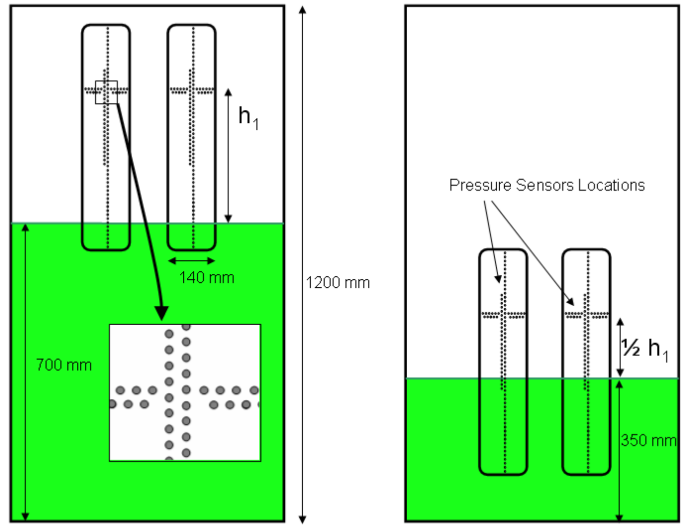


**Fig.3** – Test wall and metallic modules for the fixation of the pressure sensors at scale $s_1$ and scale $s_{1/2}$

- A high speed camera (Vision Research Phantom 7.3) is installed close to the wall in order to look closely at the impact area through the longitudinal glass wall. The camera enables a resolution of 800 x 600 pixels² at a frequency up to 6800 fps.
- Most of the time the high speed camera was used for a visualization of the free surface impacting the wall. It was focused on a longitudinal vertical plan enlighten by a continuous ion laser (Spectra-physics 0.3 W / 458-514 nm) after a fluorescein solution had been introduced into the water. In that case the high speed video recording was in the range between 1000 and 4000 fps, depending on the period of the test campaign.
- For the most interesting cases, the conditions were repeated with a Particle Image Velocimetry (PIV) measurement technique. A continuous YAG laser (Spectra-physics 5 W / 532 nm) was used and the water was seeded by 6μm diameter silver coated hollow glass spheres with a density of 1.1 g/cm$^3$. The image acquisition frequency was set to 2000 fps in that case. This set-up corresponds to a PIV technique adapted to continuous laser lighting instead of pulsed laser lighting. It was previously used successfully for flow visualizations of breaking solitons on a beach (Kimmoun *et al.*, 2009).
- The acquisition of wave probe signals was synchronized with the start of the wave maker. Video recording was synchronized with the pressure data.

## Wave maker and focalisation technique

The wave maker is moved by a hydraulic engine. The flap rotates around a horizontal axis located 40 cm under the raised bottom of the tank.

A focusing technique is used to generate a targeted wave elevation $\eta(x, t)$ at given focal distance x of the flap and time t, from a wave amplitude spectrum $a(\omega)$, $\omega$ being the rotation frequency. The flap rotation signal $\theta(x, t)$ is deduced from the spectrum thanks to the modified flap transfer function $C(\omega)$. (1)

$$\eta(x,t) = \int_\omega a(\omega)\, e^{i(\omega t - k(\omega)\, x)}\, d\omega \quad \theta(x,t) = \int_\omega \frac{a(\omega)}{C(\omega)}\, e^{i(\omega t - k(\omega)\, x)}\, d\omega$$

The integration on ω is carried out by a discretization on about 65,000 equally spaced frequencies. Figure 4 shows a wave packet generated by the flap using this focusing process.

The forced flap motions start with the small high frequency oscillations and finish with the largest low frequency wave. All wave components meet at the same time at the focal point, close to the wall, generating a large breaking wave. The focal distance between the flap and the wall is thus the main parameter to adjust the shape of the free surface just before the impact.

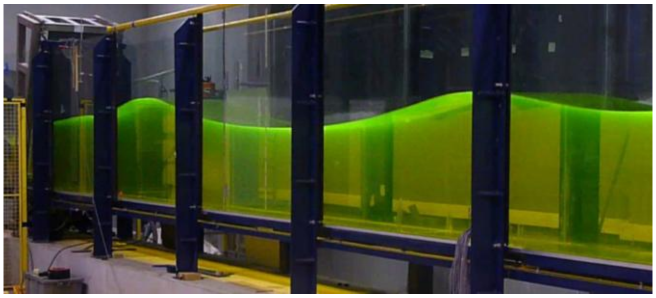

**Fig. 4** - Generation of a wave packet in ECM flume tank

When the focal point is far upstream the wall, the wave breaks before the wall. This kind of impact generates very low pressures and is not of much interest from a designer point of view. When the focal point is chosen closer to the wall, impacts with an entrapped air pocket may occur, referred to as *air-pocket impacts*. While the crest is breaking, the interaction between the wave and the wall induces a trough run-up. The air pocket is entrapped between the crest, the trough and the wall. The size of the air pocket is getting smaller when the focal point is getting closer to the wall. If the focal point is set further in the same direction, even beyond the wall, the trough run-up becomes dominant with regards to the crest momentum and no real impact occurs. This is referred to as a *slosh impact*. In between these two usual situations, there is a theoretical situation corresponding to an air pocket, the volume of which is null. This case induces a much localized flip-through of the free surface just in front of the wall. It is referred to as *flip-through impact*. The closer the situation is to the flip-through,the larger and sharper is the peak pressure.

These different kinds of waves have been studied in detail, in a larger facility, in the frame of the Sloshel project. For more information refer to Brosset *et al*., (2009). The Sloshel project was studying full scale waves with the real NO96 containment system. The scales studied in ECM must be considered for comparison purpose as scales $s_1$=1/7.5 and $s_{1/2}$=1/15.

Figure 5 shows four air-pocket impacts obtained at scale $s_1$ for four focal distances increasing progressively from 15.3 m to 15.6 m.

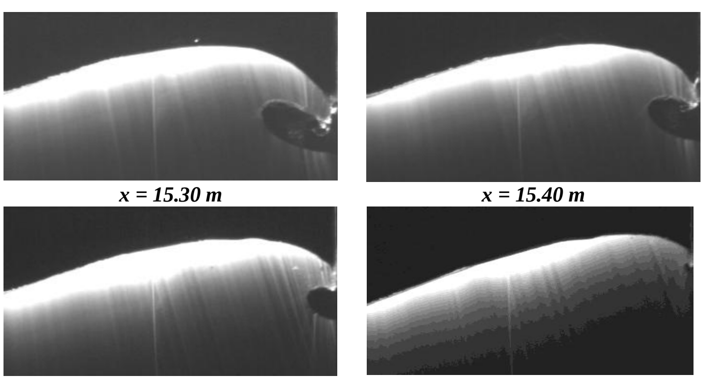

***x = 15.30 m*** ***x = 15.40 m***

***x = 15.50 m*** ***x = 15.60 m***

**Fig. 5** - Breaking wave profiles just before impacting for four air-pocket impacts corresponding to four close focal distances x at scale $s_1$

The four snapshots are given in each case at a time just before the impact. The different status in the wave breaking process is clearly observed for the four different focal distances. The sooner the breaking; the larger the air pockets.

The type of wave signals that were intended to be studied at first was the signals derived by Froude-scaling from those studied during the Sloshel project at a much larger scale. Some modifications, in order to obtain a better repeatability of the results, have been applied to these signals and are described later. The recent full scale test campaign of Sloshel project that took place in April 2010 took advantage of these improvements.

This study has been focused exclusively on the air-pocket impacts, tuning the focal point location for obtaining different sizes of the air pocket.

## REPEATABILITY OF THE GLOBAL FLOW AT A GIVEN SCALE

Without any caution, repetitions of the same wave maker signal may lead to slightly different global flows, and hence different shapes of the free surface just before impact. In that case the comparison of the impact pressures would not make sense. Figure 6 shows three repetitions of the same flap motion at scale $s_{1/2}$. The waves generated are referred to as 354, 355 and 356.

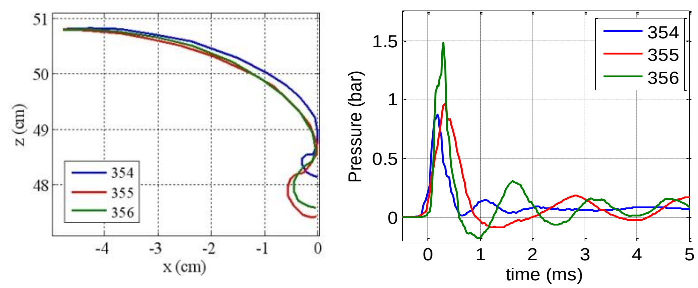


**Fig. 6** - Free surface profiles at the impact time for three different waves obtained with the same theoretical wave maker motion (left) and corresponding max pressure signals (right). Waves 354, 355 and 356

For different reasons, analysed later, the wave profiles (Figure 6 – left) obtained with the same excitation of the flap are quite different. Consequently, with no surprise, the impact pressure time traces (Figure 6 – right), given each time at the sensor getting the maximum pressure, are also significantly different.

For a relevant comparison of impact pressures after repetitions of the same wave maker command, a pre-requirement is that the global flow until the impact is the same. So, all measurements in the chain from the wave generation to the wave impact described in Table 2 must be precisely the same for the same theoretical signal of the wave maker.

**Table 2** – chain of measurements from wave maker to wall to be checked for repeatability studies

| | |
|---|---|
| **1** | Wave maker motion |
| **2** | Wave elevations at wave gauges $wg_1$, $wg_2$, $wg_3$, $wg_4$ |
| **3** | Wave surface profile at impact time |

Only after fulfilling this pre-requirement of identical global flows, will the impact pressures be compared.

Fixing, *a priori*, a minimum accuracy when comparing the wave profiles at the impact time from high speed camera pictures, would be artificial. The final comparison of the impact pressures will determine this actual accuracy, which is required on the global flow. Nevertheless, it is reasonable to consider, for instance from Figure 6, that *the order of magnitude* is the millimetre.

Two major sources have been identified as responsible of most of the discrepancies observed in Figure 6:

- The repeatability of the wave maker motions,
- The uncertainty on the water depth measurement.

## Repeatability of the wave maker motions

Repeatability of the wave maker motion for the same theoretical signal is obviously a condition for a good repeatability of the future wave development. Considering the accuracy required after the 15.5 m wave traveling, an extreme accuracy is required on the flap signals.

Figure 7 shows the wave elevations, as measured by the closest wave gauge to the wave flap (wave gauge $wg_1$ on Table 1), for the three wave repetitions shown in Figure 6 (waves 354, 355 and 356 at scale $s_{1/2}$).

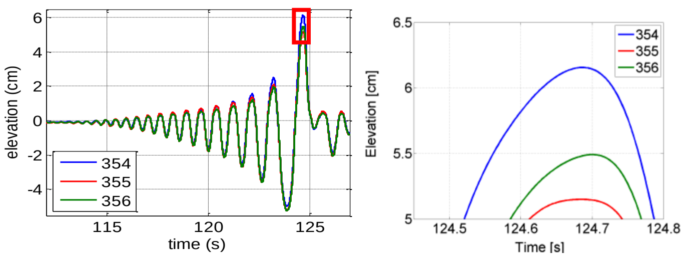


**Fig. 7** - Wave elevations from the wave gauge $wg_1$ for the three waves in Fig. 6 generated by the same theoretical wave maker signal.
Left: overview of the signal, Right: zoom-in on the highest crest

So, the discrepancies on the largest crest at wave gauge $wg_1$ at only 0.825 m of the flap are already around 10 mm. In that condition, one can obviously not reach the targeted accuracy of 1 mm at the wall level.

From the beginning of this study, it was believed that a main source of non repeatability was the high frequency content of the wave spectrum applied to the wave maker. Indeed the theoretical flap motion amplitude spectrum a(ω)/C(ω), which is derived from the wave amplitude spectrum a(ω) thanks to the transfer function of the flap C(ω), has a high frequency content that will lead to very short duration and short amplitude oscillations of the flap in time domain. The flap may not be able to follow mechanically accurately these oscillations but they have a theoretical influence on the wave profile at the wall level.

So a new wave spectrum was searched in order to replace the Sloshel spectrum $a_s(\omega)$. The *Ricker* spectrum $a_r(\omega)$ commonly used in geophysics was selected (Brinks, 2008):

$$a_r(\omega) = A_r \sqrt{T}\, e^{-\omega^m T} \left(1 - a\left(\omega^m T - 1\right)\right) \tag{2}$$

with *ω* the pulsation. Four parameters (*m, T, A, a*) enable the adjustment of the spectrum. The parameter *a* is used to determine the peak of frequency $\omega_p$ using:

$$\omega_p = e^{\frac{1}{m}\ln\left(\frac{1+2a}{aT}\right)} \tag{3}$$

Parameter *A* sets the amplitude, *m* and *T* are shape parameters of the spectrum. These parameters were fitted in order to minimize the mean quadratic difference with the *Sloshel* spectrum.

Figure 8 shows a comparison of typical wave elevation time histories at $wg_1$, just after the flap (see Table 1), for both the *Sloshel* and the *Ricker* signals.

The high frequency oscillations of the flap at the beginning of the forced motions are much attenuated with the *Ricker* signal with regards to the *Sloshel* signal. The largest waves are also affected but there is no real constraint here as far as the wave shape is relevant.

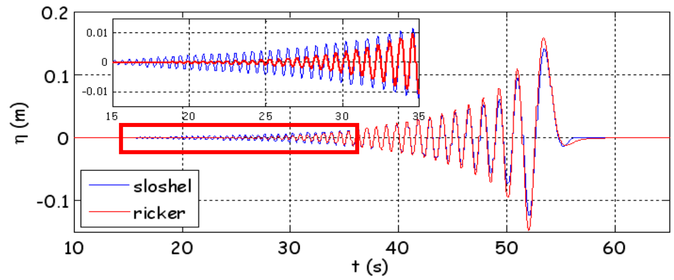


**Fig. 8** - Comparison of the wave elevations at $wg_1$ (next to the flap) for typical Ricker and Sloshel wave maker signals. Zoom-in corresponding to the red rectangle.

The results presented later in this paper have all been obtained with the *Ricker* signal. Nevertheless, the approach consisting to remove the high frequency content from the flap imposed motions should be further developed. Attempts in the time domain will be made soon within an upcoming campaign in ECM, removing directly the oscillations being too quick for the flap to be followed accurately. Figure 9 shows the initial flap amplitude derived from the *Ricker* wave spectrum and the modified signal as cut in the time domain with a relevant connection at the cut.

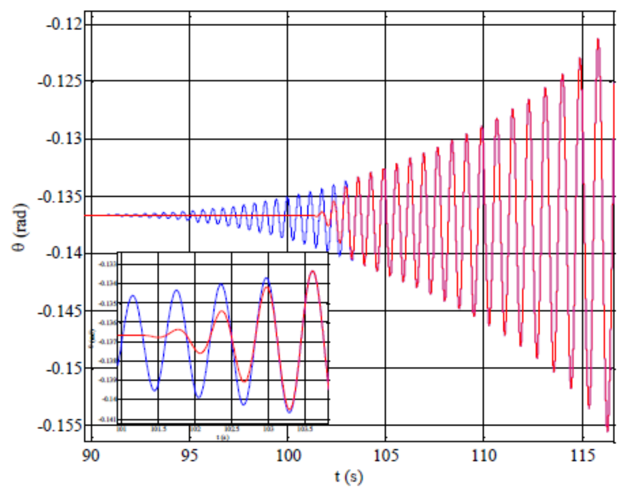


**Fig. 9** – Flap amplitude signal from a *Ricker* wave spectrum (blue) and after a time domain transformation in order to suppress the high frequency oscillations – Zoom-in in the cut area

When using the same facility at two different scales, as it was the case in ECM, the need for removing the high frequency content from the water maker excitations increases because the frequencies of the flap oscillations have to be higher at small scale for complying with the Froude similarity.

## Uncertainty on the water depth (step 1)

The water depth is also a sensitive parameter. Indeed the water depth h is very much linked to the focal distance x. The theoretical flap motions θ(x, t) is calculated in order to fit with a focal distance adapted to a given flume length D and a given water depth h. When the scale is fixed, the ratio h/D is fixed. If h is not accurately measured, being unknowingly (h+δh) instead of h, and the flap signal is kept the same, the wave packet will be differently focused. A (too) simple reasoning consists in considering the real focal distance at (x+δx) such as the scale is kept the same: (h+δh) / (x+δx) = h/x. Thus, δx = δh•x/h. If the uncertainty on the water depth is δh = 1 mm, it means an unknown shift of the focal point of δx = 0.0014•x at scale $s_1$ and half this value at scale $s_{1/2}$. For a focal distance x = 15.3 m, the shift becomes δx = 22 mm.

The four snapshots of Figure 5 obtained for focal distances shifted regularly of 10 cm gave an idea of what kind of wave profile discrepancy could be expect with a 2 cm shift.

Figure 10 shows the wave profiles just before impact for four different water depths increasing by step of 1 mm from 34.9 cm.

So, the uncertainty on the water depth is to be considered also as an amplified uncertainty on the focal distance.

This influence is obviously especially important when working around the focal distance corresponding to the flip-through area, as this phenomenon is very sharp.

The water depth has another major influence on the ability for a given network of sensors to capture phenomena that may induce strong gradient of pressures over the distance between two consecutive sensors. This particular issue is addressed in a next sub-section.

The water depth should thus be measured with a special care, when the flume is totally at rest, which requires a long waiting time between tests in order to ensure that the first mode of the tank is totally damped.

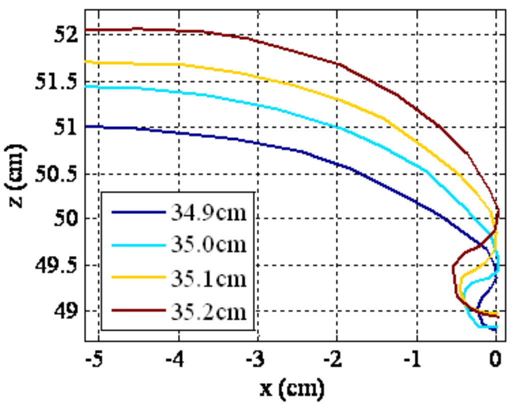


**Fig. 10** - profiles of breaking waves just before impacting for four different water depths and the same wave maker signal

A laboratory flume like ECM's is absolutely watertight: no leakage is to be accounted for. Nevertheless the evaporation cannot be avoided and leads to significant change of the water fill level over a day or a night with regards to the accuracy targeted.

This phenomenon could explain the discrepancies that are observed when comparing the last run of a day (e.g. run 354) and the first run of the next day (e. g. run 355). The runs 354 and 355 selected in Figure 6 illustrate this evaporation consequence.

So, repeatability for a target focal distance must be performed over a short period of time (a few hours) in order to avoid any tiny change of water depth by evaporation.

### Repeatability of the global flow (results)

When comparing repetitions of the Ricker signal in a short period of time, a good repeatability of the global flow has been obtained at both scales for different focal distances leading to repeatable different sizes of gas-pocket impacts.

**At scale $s_{1/2}$**, four tests carried out in a row, the same day as run 355 but later have been selected. They correspond to a small gas pocket. Figure 11 shows the four superimposed wave profiles just before impact.

**At scale $s_1$,** two tests (124 and 125), performed one after the other in a short period of time, have been selected. They correspond to a small gas-pocket impact.

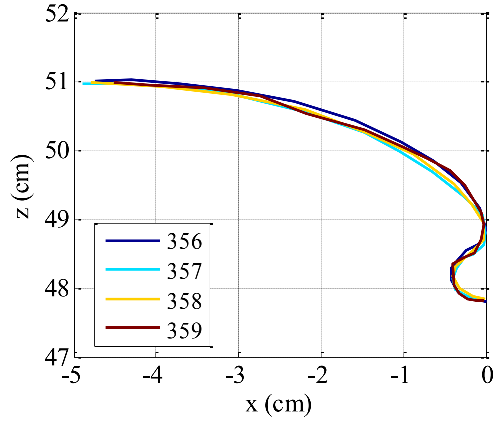


**Fig. 11** -. Wave profiles for four repetitions of the same flap signal. – Scale $s_{1/2}$

Figure 12 illustrate the good repeatability obtained on the wave elevations time traces measured by the gauges $wg_3$ and $wg_4$ (see Table 1). It can be observed that the signals superimpose very accurately.

Figure 13 shows the pictures recorded by the high speed camera just before the impact. A superimposition of the snapshots is presented. The results match perfectly.

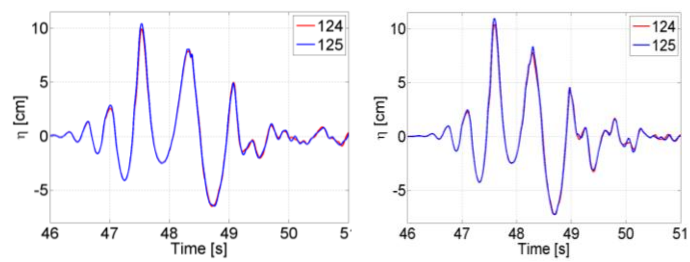


**Fig. 12** - Wave elevation time traces at $wg_3$ (left) and $wg_4$ (right) for two repetitions of the same wave maker signal at scale $s_1$. Tests 124 and 125

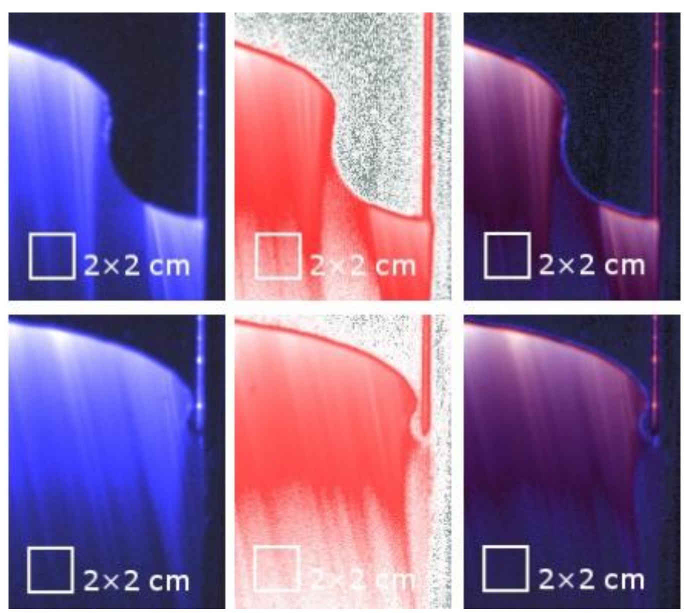


**Fig. 13** – High speed camera shots at 11ms (top) and 2ms before impact (bottom) for two repetitions of the wave maker signal (same as in Fig. 12. Run 124 (red) - Run 125 (blue) – overlaid (violet)

REPEATABILITY OF RELEVANT PRESSURE MEASUREMENTS FOR SAME GLOBAL FLOWS

Assuming good repetitions of a global flow has been obtained at a given scale, shown by accurate repetitions of the parameters of Table 2, it might be relevant to compare the impact pressures. New difficulties rise then, one has to be aware of.

Even restricted to the study of air-pocket impacts, unilateral wave impacts in a flume are able to generate very sharp pressure loads both in time and space in two different situations:

- For large air pocket impacts at the crest level (crest impact of a breaking wave).
- For small air-pocket, a sharp flip of the free surface enables locally a quick turn of the velocities from horizontal to vertical direction.

These sharp pressure peaks cannot be disregarded. Indeed Sloshel project (see Bogaert, Léonard, Marhem, Leclère & Kaminski, 2010) has shown, by means of full scale wave impact tests in a flume, that the structure of the NO96 membrane containment system used for LNG ships responds highly to such sharp pressure excitations.

This section describes how far the sharpness of these peak pressure signals is captured in space by the network of sensors shown in Figure 3 and in time by the acquisition sampling frequency.

Obviously, at the crest level for large air-pocket events or for small air-pocket impacts, only when the sharp peak pressures are captured, is the repeatability requirement relevant.

## Large air-pocket impacts

For large air-pocket impacts, the crest hits first the wall leading to localized sharp pressures. In that case, the momentum of the crest is not overcome by the trough run-up.

Figure 14 shows the development of a gas pocket impact through different snapshots separated by a time step of 5 ms. Impact of the crest confines the air-pocket, which is compressed horizontally against the wall by the liquid pushing behind, and vertically by the trough run-up.

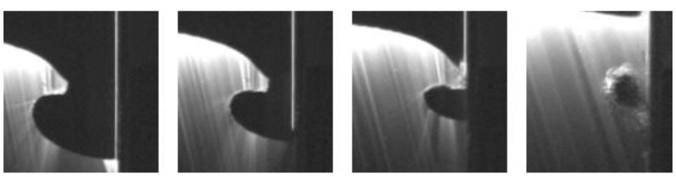

**Fig. 14** - Snapshots of a gas pocket impact at four instants: t = -10 ms, -5 ms, 0 ms and 5 ms - Time aligned on max pressure at the crest level - Scale $s_1$

The pushing liquid and the stiffness of the gas pocket act in an antagonist way very similar as a mass/spring system leading to oscillations of the gas pocket. The pressure is uniform into the gas pocket and two sensors completely entrapped in it measure exactly the same pressure. The pressure evolution into the pocket is totally determined by the evolution of its volume through the equation of state.

Figure 15 shows the pressure signature of such an impact, focusing on the crest level located at around 99 cm above the bottom. The pressure sensor at 99 cm captured a sharp peak pressure which corresponds to the crest impact. After the decay of the sharp peak, the pressure in the crest oscillates with the same frequency as seen by the pressure sensor located 1 cm below, which is inside the pocket. The oscillation period is around 8 ms. The sharp peak is captured by one sensor but not by the sensors at 1 cm above or at 1 cm below. The gradient of pressures is, thus, very high over a distance of 1 cm.

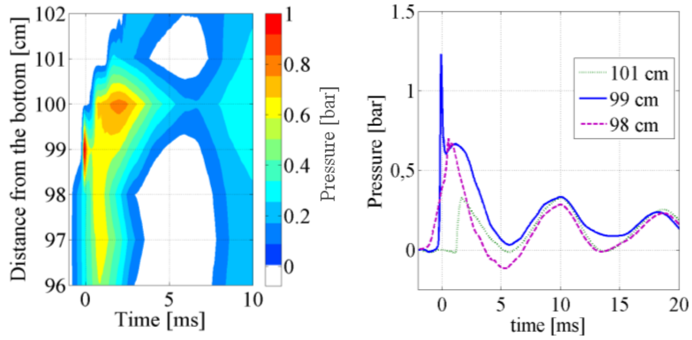


*Vertical pressure profile evolution* *Pressure signals for 3 sensors close to the crest*

**Fig. 15** – Pressure signature of an air-pocket impact at the crest level – Scale $s_1$

For all large air-pocket impacts, the crest impact is necessarily present. However, there are some for which no sharp peak can be detected by the pressure sensors. It means thus that the peak has not been captured, it does not mean that it does not exist. In that case, only the air pocket pressure is measured. The measurement may be more easily repeatable but the fact remains that the pressure measurement is not relevant.

## Small air-pocket impacts

Small air-pocket impacts behave differently than large ones. When considering air-pocket impacts with progressively smaller pockets, there is a threshold from which the trough run-up becomes dominant with regards to the crest momentum. The free surface has to flip sharply just in front of the wall. The horizontal momentum of the pushing liquid behind the remaining pocket is thus abruptly transformed to vertical momentum added to the trough run-up, which becomes a violent vertical jet. The crest is not strong enough to prevent this run-up development.

Figure 16 shows the evolution of a small air-pocket impact. Four snapshots from the high-speed camera at instants separated by 5 ms are given. The velocity fields as determined by the PIV technique, is superimposed to the camera pictures.

Large velocities can be observed at the crest level just before the impact. Maximum velocity recorded is 7 m/s. From the successive locations of the trough and of the tip of the crest, it can be noticed that the wave trough is accelerating and its vertical velocity becomes higher than the horizontal velocity of the crest. Unfortunately the trough is in a shadow area of the PIV.

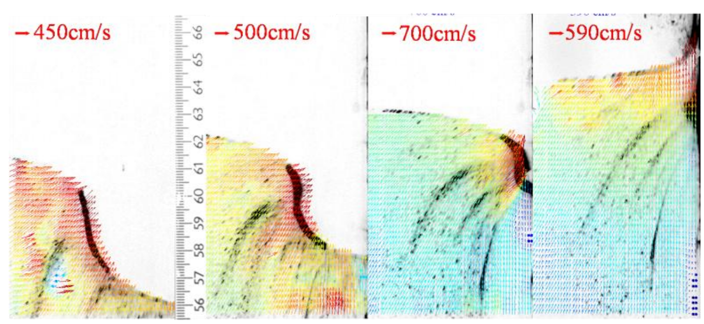


**Fig. 16** – Negative snapshots with velocity field of a small gas pocket impact at four instants: t=-10 ms, -5 ms, 0 ms and 5 ms - Time aligned on max pressure at the crest level - Scale $s_1$ - Colour scale from light blue to dark red. Dark red for the max velocity reported in each picture.

Figure 17 shows the pressure signature recorded by the sensors in the impact area.

For this type of small gas-pocket impact, the pressure signature is very different than for larger air-pocket impacts. The maximum pressure is higher (here 6.3 bar) but is still restricted to a very small area. Over the distance of 5 mm, the pressure decrease is about 4 bars.

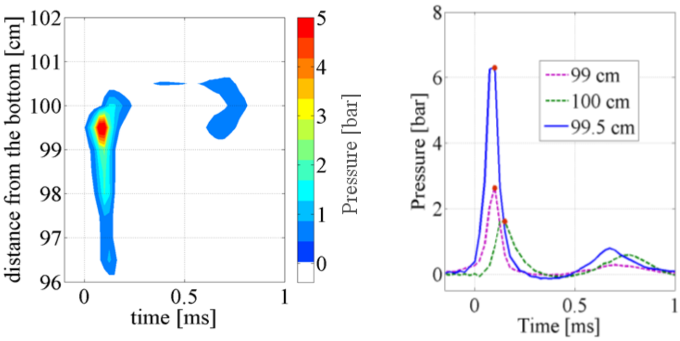


*Vertical pressure profile evolution* *Pressure signals for 3 sensors close to the crest*

**Fig. 17** – Pressure signature of a small air-pocket impact – Scale $s_1$.

There are still oscillations of the signal, but very quickly damped, showing that a small fraction of gas remained entrapped. Consequently, the frequency of the oscillations becomes very high (about 0.7 ms). The time duration of the peak is around 0.25 ms. When studying small air-pocket impacts, the volume of air pockets, hence the frequency of the oscillations and the maximum impact pressures are very sensitive to variations of the focal distance.

Table 3 shows the results of a sensitivity study at scale $s_1$. The focal distance varies from 15.57 m to 15.62 m with a minimum step of 1 cm. The focal distance 15.62 m corresponds to a *slosh impact*. In that case there is no gas pocket. For a variation of the focal distance of the order of a centimeter, impact characteristics vary very sharply.

**Table 3** - Sensitivity to the focal distances for small gas pockets

| **Focal (m)** | **15.57** | **15.59** | **15.60** | **15.62** |
|---|---|---|---|---|
| **width (cm)** | 7.63 | 3.29 | 1.62 | No |
| **Frequency (Hz)** | 160 | 440 | 1040 | No |
| **Pressure (bars)** | 1.80 | 5.41 | **6.45** | 1.55 |

## Uncertainty on the water depth (step 2)

The uncertainty on the water depth determination has already been addressed in the previous section for its influence on the global flow. At the same time, considering the high gradient of pressures that can be expected locally, the uncertainty on the fill level makes the relative location of the sensors with regards to the highest pressure area uncertain, bringing thus a new uncertainty on the pressure measurement.

A short sensitivity study on the water depth has been carried out at scale $s_{1/2}$. Four runs have been performed for increasing depths from 34.9 cm to 35.2 cm by steps of 1 mm. As the variations on the water depth are here considered as uncertainties, these differences are normally unknown by the experimenter who would apply a nominal signal to the wave maker. So, the wave maker signal is kept the same for the different water depths studied. It corresponds to a focal distance of 7.765 m. If the ratio of the focal distance to the depth is considered, a 3 mm variation on the depth corresponds to a 66 mm variation on the focal distance.

Results are reported in Table 4 in terms of maximum width of the gas pocket, frequency of its oscillations and maximum pressure on all sensors.

**Table 4** - Sensitivity study of the water depth for a given flap signal – scale $s_{1/2}$.

| **Depth (cm)** | **34.9** | **35.0** | **35.1** | **35.2** |
|---|---|---|---|---|
| **width (cm)** | 0.38 | 0.50 | 0.69 | 0.91 |
| **Frequency (Hz)** | 1125 | 930 | 870 | 570 |
| **Pressure (bar)** | 0.740 | 1.383 | 1.423 | 2.075 |

The profiles of the breaking waves just before impact have already been shown in Figure 10.

The two different influences of the water depth are clearly seen in Table 4. The influence on the global flow is observed through the width of the air pocket and consequently through the frequency of its oscillations. For decreasing widths of the pockets, the maximum pressures should normally increase. Here the opposite trend is observed, showing the second effect of the water depth change: the fit of the pressure sensor location giving the maximum pressure is getting progressively worse and worse with regard to the crest location when passing from a water depth of 35.2 cm to 34.9 cm. However the bad repetition of the global flow should not enable a comparison of the pressures.

**The quantity of dissolved air into the water** plays also obviously a role on the quality of the repetitions during the few days after refilling the tank. During this period, the water is moved by the flap and by the impacts, the amount of dissolved air decrease and reach a constant value. No sensitivity study has been performed yet to quantify the influence of this parameter but all tests have been performed with the same water.

## Technical ability to capture the sharp peak pressures

How far can the sharp peak pressures that occur at the crest of large air-pocket impacts or for small air-pocket impacts be captured?

**In space**, it has been shown that the gradient of pressure can be very large over a distance of 5 mm. The diameter of the sensors is 5.5 mm and the staggered locations of the sensors every 5 mm enables to have almost a continuum of pressure sensors in the vertical direction '(see Figure 3). So, theoretically, even a sharp peak of pressure should, most of the time, not be missed. Nevertheless, just a tiny change in the location of the crest with regards to the sensor location should modify much the measurement. If the pressure hot spot is covered by the area with the two horizontal lines of sensors, it should not be missed.

**In time**, one can wonder whether the sampling frequency is sufficient or not. Figure 18 shows zoom-ins of the maximum pressure area for the signals obtained respectively in Figure 15 for large air-pocket impacts at the crest level and in Figure 17 for small air-pocket impacts. The dots represents the sampled times.

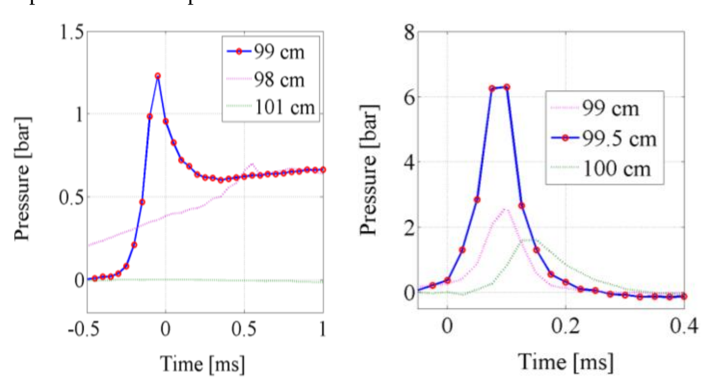


*Large-pocket impact of Fig. 12 Sensor at 99 cm* *Small pocket impact of Fig. 14 Sensor at 99.5 cm*

**Fig. 18** – data acquisition sampling of the pressure signals at small and at large air pocket impacts. - Sampling frequency f = 40 kHz – Scale $s_1$

The sampling frequency of 40 kHz adopted for all tests enables to discretize adequately the sharpest pressure signals obtained.

### Repeatability of the pressure measurements at each scale

It has been shown that the high density of sensors used (distance minimum of 5 mm) together with their rather large diameter (5.5 mm) should enable to capture spatially the sharp pressure peaks obtained for local crest impacts of large air-pocket events or for small air pocket impacts. The maximum pressure recorded is an average on the sensor diameter. As far as repeatability is concerned the governing parameter is the accurate location of the pressure hot spot with regards to the locations of the pressure sensors and especially to the two staggered horizontal lines of sensors shown in Figure 3. So with an accuracy of 1 mm on the wave profile just before the impact at scale s1 (global flow), and with repetitions in a short period of time (no change in the water depth) good repeatability of the pressures is achievable.

Two examples are given corresponding to scales s1 and s1/2.

**At scale $s_{1/2}$** four tests performed during the same day have been selected. They correspond to tests 356 to 359 that proved to have very similar global flows (see Figure 11). Figure 19 shows the pressure time traces obtained from the sensor recording the maximum pressure.

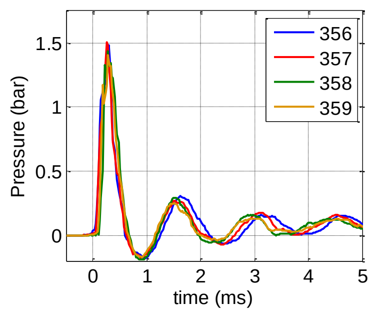


**Fig. 19** - Pressure traces at the same location for four repetitions of the same flap signal. Wave profile before impact in Figure 11

These tests correspond to a small gas-pocket impact. The frequency of the gas pocket oscillations is 700 Hz. The frequency range obtained during the tests at scale $s_{1/2}$ is between 225 Hz and 715 Hz. Therefore, these tests correspond to a size of gas pocket close to the smallest obtained during the tests at scale $s_{1/2}$. A very good repeatability of the pressure time traces was obtained.

**At scale $s_1$,** two tests (124 and 125), performed also one after the other in a short period of time, have been selected. They correspond also to a small gas-pocket impact. The repeatability of the global flow has already been shown in Figures 12 and 13. The repeatability of the impact pressure measurement is illustrated in Figures 20 and 21.

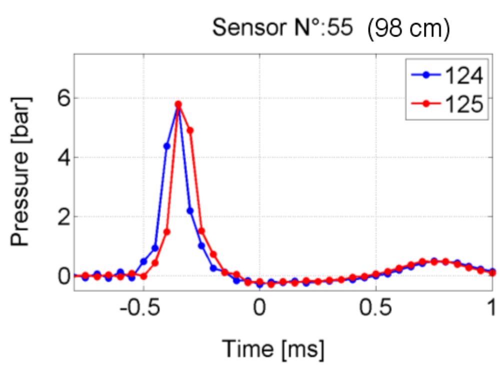


**Fig. 20** – Pressure time traces given by sensor n°55 for two repetitions of the wave maker signal. Test 124 (blue), test 125 (red) – Scale $s_1$

Figure 20 presents the pressure time traces obtained by a representative sensor located in the high pressure area. Figure 21 shows the time evolution of the pressure profile along the wall.

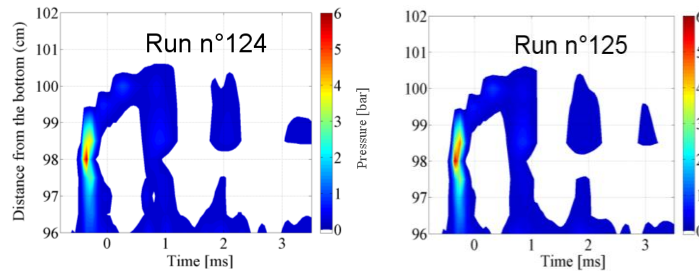


**Fig. 21** – Time evolution of the pressure profile along the wall for two repetitions of the wave maker signal. Test 124 (left), Test 125 (right) – Scale $s_1$

These two tests generated high pressures peaks. An accuracy of 3% was nevertheless obtained on the repetition of the pressure peaks.

So, a good repeatability of the pressure peak measurements is achievable. It requires challenging conditions:

- a good repeatability of the wave maker motions that can be facilitated by removing as far as possible the high frequency content of the wave spectrum
- a dense repartition of sensors in the hot spot area in order not to miss very localized high pressure zones
- no variation of the water depth, which requires to perform the tests consecutively in a short period

During the whole test campaign covering almost 400 tests. At each scale, only a few series fulfil all the requirements. Many waves have been performed with a good repetition of the global flow but with a pressure hot spot outside the dense covering of the sensor configuration.

## SIMILARITY AT BOTH SCALES

In the previous section, it has been shown that a good repeatability of the pressure measurements can be achieved when challenging precautions are fulfilled. Now, a second requirement for a deterministic comparison of pressures at two different scales (see introduction) is a good similarity of the global flows at the two scales for the different conditions studied. According to the theory, the global flow should be similar if the wave maker signals are Froude-scaled. So, the accurate scaling of the flap signal is addressed in this section. Then the issue of the pressure diameter scaling rises.

### Wavemaker signal scaling

With the rotational wave maker there is a potential difficulty to apply the Froude-scaling that is to be studied carefully for a good similarity of global flows.

The scaling process for the flap signal can be described as follows:

- The starting point is the Ricker spectrum ar(ω) and the transfer function of the flap C(ω)
- From these data are deduced the elevation of the free surface $\eta(x_1, t_1)$ and the rotation of the flap $\theta(x_1, t_1)$ at scale $s_1$, where $x_1$ is the location of the focal point and $t_1$ is the time (see formula (1))
- By Froude-scaling the free surface elevation one obtains:
  $\eta_{1/2}(x, t) = \eta(x_{1/2}, t_{1/2})$ at scale $s_{1/2}$
- From $\eta_{1/2}$ and the transfer function of the flap we deduce the rotation signal of the flap at scale $s_{1/2}$: $\theta_{1/2}(x, t) = \theta(x_{1/2}, t_{1/2})$

When applying directly this process, very similar waves are created at both scales in terms of free surface elevation, as measured by the last wave gauges $wg_4$ before the wall (see Table 1). Nevertheless these small discrepancies induce different free surface profiles just before the impact and the comparison of the pressures at both scales in these conditions is not relevant.

Figure 22 illustrates these discrepancies at both scales for a representative example of wave signal generating a gas pocket impact.

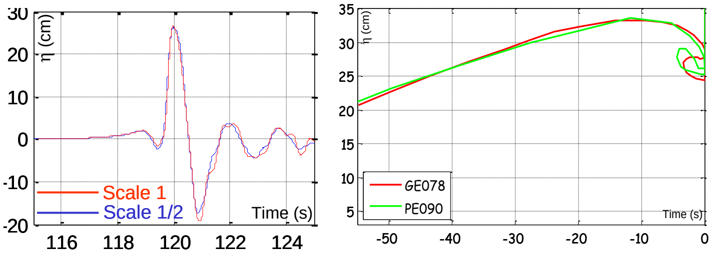


*Histories of the wave elevation. Scale s½ is Froude-scaled* *Free surface profiles just before the impact (from high speed camera)*

**Fig. 22** - Comparison of waves generated at scale $s_1$ and scale $s_{1/2}$ by Froude-scaled wave maker signals without function transfer correction

Actually, this theoretical scaling process is spoiled by the transfer function of the flap which does not allow an accurate scaling of the wave elevations for the low frequency waves. A correction of the flap transfer function for the low frequencies is necessary.

Figure 23 shows the comparison at both scales of the wave elevation spectra at wg1 just in front of the flap (see Table 1) before and after the low frequency correction of the transfer function using the same signal at scale $s_1$ that was used in Figure 22.

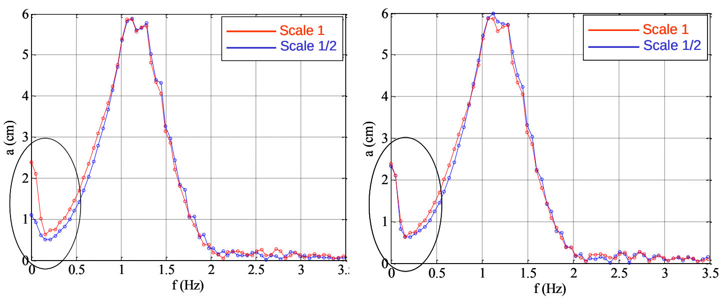


*Without correction of the wave maker tranfer function* *With correction of the wave maker transfer function*

**Fig. 23** - Comparison of wave elevation spectra at $wg_1$ at scale $s_1$ and scale $s_{1/2}$ obtained by Froude-scaled wave maker signals

After low frequency correction of the transfer function the profile of the free surface looks very similar at both scales until the impacts as shown in Figure 24 at two different instants.

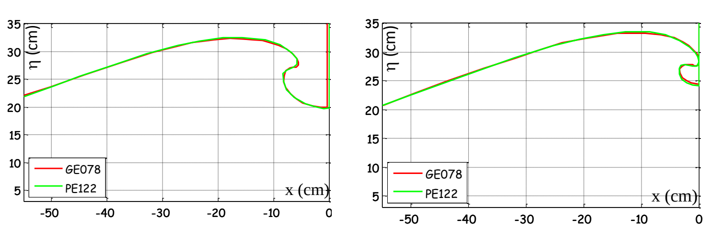


*Profiles of the free surface at 5 ms before the impact* *Shapes of the free surface just before the impact*

**Fig. 24** - Comparison of wave profiles generated at scale $s_1$ and scale $s_{1/2}$ by Froude-scaled wave maker signals after function transfer correction (profiles plotted from high speed camera pictures)

### Pressure spatial interpolation

Even when the flows are Froude-similar at both scales, the comparison between the pressures is spoiled by the fact that the pressure sensors used at both scales are the same. Therefore, the size of the pressure sensitive area is not scaled as it should be. Considering the sharp pressure peaks recorded this would lead to a bias if no correction was applied.

The PCB sensors record an instantaneous average pressure over a disk of a 5.5 mm diameter. For correcting this potential bias, the pressure signals on the hot spot areas at scale $s_1$ should be reconstructed by interpolation, as though they were recorded by virtual sensors of 11 mm diameter.

## COMPARISON OF THE GAS-POCKET PRESSURES AT BOTH SCALES

### Relevance of the data for the high peak pressure comparison at both scales

From the previous sections we can draw the following conclusions:

- An accurate repeatability of the global flows has been achieved at each scale with the Ricker signal when the series of tests have been performed in a short period of time enabling to keep precisely the same fill level. The wave profiles just before the impact looked very similar when the same flap signal was used. An accuracy of less than one millimetre was obtained. This achievement was made technically possible by a reduction of the high frequency content of the wave signal.
- When good repetitions of the global flow have been achieved and when the very sharp pressure peaks induced either by the crest impacts of large air-pocket events or by small air-pocket impacts have taken place right in the area densely covered by the pressure sensors (see Figure 3), a good repeatability of these sharp pressure time traces has been obtained. An accuracy of a few percents on the peaks was obtained. This achievement was made possible by a dense repartition of sensors and a high sampling frequency (40 kHz).
- After correcting the flap transfer function in the low frequency area, a good similarity of the global flow was achieved at both scales for Froude similar wave maker signals
- Around 400 hundred tests have been carried out during this campaign (for both scales). Many tests have been used in order to tune the different parameters. A few series of repeatable global flows have been obtained at each scale. Some of them, at each scale, give repeatable pressures in the hot spot area. Just a few couples are in good similarity of the global flow at both scales. None of them are available for a relevant pressure comparison in the hot spot area. The few couples giving similar global flows turned out not to be relevant because the location of the hot spot did not match the high density area of sensors.

It is thus impossible to compare directly impact pressures in the hot spots areas from the data base that has been built yet. However, all lessons learned during this campaign and good results obtained at each stage make possible this deterministic comparison in a very near future.

As the pressure inside an air pocket and the associated frequency is easier to capture reliably, a comparison is proposed between both scales, restricted to these parameters.

### Basis for a relevant comparison at both scales

The natural parameter enabling to sort out the different air-pocket impacts at both scales should be the focal distance. However, it has been shown how a small uncertainty on the water depth can lead to a large uncertainty on the focal distance and more generally on the Froude-similarity of the flap steering signals.

In the following, a comparison is proposed at both scales, limited to air pocket impacts that have geometrically similar areas of gas entrapped in a vertical plane, when the pocket is closing. More precisely, the reference time for the comparison of the pocket surface at both scales is the time for which the pressure at the crest level is maximal. This instant is so close to the time of first contact that it is considered that the surface of the pocket remains the same in between. At that moment, when the gas is just entrapped, the pressure inside both gas pockets is assumed as the atmospheric pressure.

The pocket surface is derived from pictures captured by the high speed camera as presented in Figure 5, 13 and 14. The accuracy is clearly getting smaller when the size of the gas pocket is smaller. This is especially due to the use of the powerful laser lighting, which induces an overexposure on the pictures near the free surface in the meniscus vicinity.

The instant when the pocket is closing corresponds to the end of the global flow (assumed to be Froude-similar at both scales) and to the beginning of the local interactions between the wave, the gas and the wall including the compression of the gas pocket. The study focuses now on the pocket compression at both scales.

When the maximum pressure is reached at the crest level, the pressure inside is still the atmospheric pressure. So, it makes sense to compare pockets that are geometrically similar at that time instance because these pockets have scaled quantities of entrapped gas. Global quantities like the gas pocket pressure, the frequency of its oscillations depend on the interaction between the compressing flow around the pocket and the resisting compressed gas, acting like a mass-spring system. For geometrically scaled initial pocket surfaces, the global flow is close to be Froude-similar but the discrepancies are not well bounded. On the other hand, the compressibility of the gas is the same at both scales and hence is not scaled properly as stated in Braeunig *et al.*, (2009). So, one would like to check as far as possible, whether this leads to a compressibility bias or not.

## Comparison of the air pocket parameters at both scales

The pressure within the air pocket and the frequency of oscillations are compared at both scales for geometrically scaled surfaces of the air pockets.

Figure 25 shows the results for the pressures. Figure 26 shows the results for the frequencies. Each Figure is cut into two parts. On the left side, the raw data are presented at both scales without any scaling for the results at scale $s_{1/2}$, so that the same volume of gas pockets is considered at both scales. On the right side, the following factors are used for scaling from $s_{1/2}$ to $s_1$: a factor $\lambda^2 = 4$ for the surfaces, a factor $\sqrt{\lambda} = \sqrt{2}$ for the pressures and a factor of $\lambda = 2$ for the frequencies.

The frequencies have been determined by two different methods: by calculating two consecutive maximums of the pressure time traces and by a spectral method. The results have been considered as valid when the two methods matched. Without surprise, it can be observed that, whatever the scale, the maximum pressure inside the pocket decreases regularly when the surface of the pocket increases.

The quality of the dots alignment on the figures shows also how far the measure of the parameters (pressure or frequency) can be considered as deterministically defined. Surprisingly, this quality is clearly higher at scale $s_{1/2}$ than at scale $s_1$. This is due to the fact that most of the tests at scale $s_{1/2}$ have been performed at the end of the campaign applying a more severe testing protocol because of the experience gained.

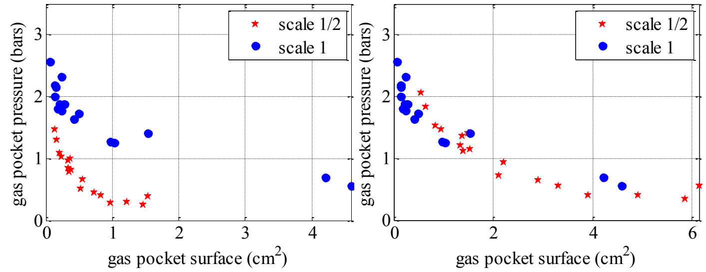


*Raw data without scaling*

*At scale $s_1$/2, surface scaled by 4 and pressure scaled by √2*

**Fig. 25** – Maximum pressure inside the air pocket vs. the air pocket surface for scales $s_1$ (blue) and $s_{1/2}$ (red). Without scaling (left) and with scaling (right)

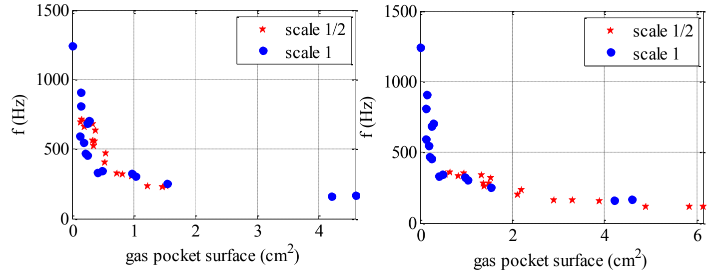


*Raw data without scaling*

*At scale $s_1$/2, surface scaled by 4 and frequency scaled by √2*

**Fig. 26** – Frequency of the air pocket oscillations vs. the air pocket surface for scales $s_1$ (blue) and $s_{1/2}$ (red). Without scaling (left) and with scaling (right)

It is also apparent that most of the tests have been performed with the same range of air-pocket actual sizes at both scales, therefore without a good match after scaling the surfaces. This range is limited by the resolution of the pictures for small sizes and by the Ricker wave spectrum that has been chosen for the large sizes.

When comparing the results on the left sides of Figures 25 and 26, namely comparing the same size of air pockets at two different scales, the maximum pressures scale approximately with $\lambda = 2$ whereas the frequencies are kept approximately the same. As the stiffness of the gas pockets are the same, this result means that the added masses of liquid around the pocket volume (the equivalent mass of the pushing liquid in a 1D mass-spring model) are also approximately the same, while the velocities of the global flows are Froude-scaled. Nevertheless, this comparison, although academically interesting, does not make sense for gaining insight about sloshing model tests, as the global flows are not Froude-similar at both scales.

The only relevant way to compare the pressures and frequencies at both scales is for geometrically scaled volumes of air-pockets considering similar global flows, namely as presented on the right sides of Figure 25 and 26. The trend is then a scale factor of $\sqrt{\lambda} = \sqrt{2}$ for the pressures and a factor of $\lambda = 2$ for the frequencies. It means that when the compression of the gas begins, a bias starts to develop, both in space and time, with regards to a Froude similarity (scale factor of $\lambda$ for the pressures and $\sqrt{\lambda}$ for the frequencies).

The compressibility bias described in Braeunig *et al.*, (2009) is experimentally confirmed.

The conclusions on the scaling for gas pocket impacts must unfortunately not ne generalized. In a parallel study related to the Sloshel project, Bogaert, Brosset, Léonard, Kaminski (2010), obtained a scaling factor of $\lambda$ for both the pressures and the frequencies when comparing carefully gas pocket impacts at scale 1 and 1:6. A simple 1D semi-analytical model of the air-pocket compression enables to explain both results despite the apparent contradiction.

## CONCLUSIONS

A relevant deterministic comparison of impact pressures at two different scales is achievable by means of wave impact tests in a flume tank, even when comparing sharp peak pressures induced by the wave crest for large air-pocket impacts or by small air-pocket impacts. However this goal was only partially reached during the test campaign performed in ECM at two scales ($s_1 = 2\ s_{1/2}$). Although all challenging requirements for such an objective were fulfilled separately, no couple of impacts was relevantly comparable at both scales for sharp pressure pulses. Only the more easily *graspable* air-pocket parameters (pressure and frequency of oscillations) were possible to compare.

The reduction of the low frequency content of the wave maker steering signals enabled to obtain accurately repeatable signals and therefore accurately repeatable global flows until the last moment before the impact, provided that tests were repeated in a short period of time for which the water depth could be assumed as constant. Repeatable global flows led to repeatable impact pressure measurements even in case of sharp peak pressures, provided that the pressure hot spots were adequately covered by a high density of sensors and the acquisition sample frequency was sufficiently high. Finally the Froude similarity of the global flows was also achieved when correcting the transfer function of the flap wave maker in the low frequency region.

Despite the uncertainties, the comparison of the pressures inside air pockets and of the frequency of their oscillations with regards to the air-pocket volume, gave certain trends for possible scaling factors. The scaling factor for the pressures turned out to be $\sqrt{\lambda}$, the scaling factor for the frequencies is $1/\lambda$. This confirms experimentally the compressibility bias highlighted theoretically and numerically by Braeunig *et al.*, (2009).

Nevertheless the scaling factors obtained must not be considered as general. Another parallel study conducted in larger flume tanks (Bogaert *et al.*, 2010) concluded to the same frequency scaling factor but a pressure scaling factor of $\lambda$. Both results, although apparently in contradiction, match well with a simple 1D analytical model of a gas pocket compression developed by Bogaert *et al*.

## REFERENCES

Brinks, R., (2008). "*On the convergence of derivatives of B-splines to derivatives of the Gaussian function"*, Comp. Appl. Math., 27, 1, 2008.

Bogaert, H., Brosset, L., Léonard, S., Kaminski, M., (2010), "*Sloshing and scaling: results from Sloshel project*", 20th (2010) Int. Offshore and Polar Eng. Conf., Beijing, China, ISOPE.

Bogaert, H., Léonard, S., Marhem, M., Leclère, G., Kaminski, M., (2010). "*Hydro-structural behavior of LNG membrane containment systems under breaking wave impacts: findings from the Sloshel project*", 20th (2010) Int. Offshore and Polar Eng. Conf., Beijing, China, ISOPE.

Braeunig, J.-P., Brosset, L., Dias, F., Ghidaglia, J.-M., (2009). "*Phenomenological study of liquid impacts through 2D compressible two-fluid numerical simulations"*, 19th (2009) Int. Offshore and Polar Eng. Conf., Osaka, Japan, ISOPE.

Braeunig, J.-P., Brosset, L., Dias, F., Ghidaglia, J.-M., Maillard, S., (2010). *"On the scaling problem for impact pressure caused by sloshing"*, to be submitted to a scientific journal (May, 2010?).

Brosset, L., Mravak, Z., Kaminski, M., Collins, S., Finnigan, T., (2009) *"Overview of Sloshel project"*, 19th (2009) Int. Offshore and Polar Eng. Conf., Osaka, Japan, ISOPE.

Kimmoun O., Malenica ·S., & Scolan Y.M, (2009). *"Fluid structure interactions occuring at a flexible vertical wall impacted by a breaking wave"*, 19th (2009) Int. Offshore and Polar Eng. Conf., Osaka, Japan, ISOPE.